High-Stable Covalent Organic Framework Towards Palladium Removal from Nuclear Wastewater

Wenchen Song , Junli Wang * , Wentao Wang , Hui Wang , Yao Liu

Posted Date: 8 April 2025

doi: 10.20944/preprints202504.0436.v1

Keywords: High-level liquid waste; platinum group metals; COF-42; Palladium; adsorption

 doi:10.20944/preprints202504.0436.v1

Article

High-Stable Covalent Organic Framework Towards Palladium Removal from Nuclear Wastewater

Song Wenchen [1], Wang Junli [1,2,*], Wang Wentao [1], Wang Hui [1] and Liu Yao [1]

[1] Department of Radiochemistry, China Institute of Atomic Energy, 102413 Beijing, China

[2] State Key Laboratory of Chemical Resource Engineering, College of Chemical Engineering, Beijing University of Chemical Technology, Beijing 100029, China

* Correspondence: yanthcn@163.com or lijw@mail.buct.edu.cn

Abstract: The proper management of High-Level Liquid Waste (HLLW) is essential for safeguarding the environment and human health. The presence of platinum group metals (PGMs) in HLLW can impact its disposal due to their high melting points. Therefore, it is vital to eliminate PGMs during the initial treatment phase. Thus, this research introduces an adsorption method using COF-42 as an adsorbent to target palladium (Pd). The molecular structure, integrity, and morphology of COF-42 and Pd@COF-42 are thoroughly assessed using various techniques such as PXRD, FT-IR, TGA, XPS, and SEM. The study further investigates the adsorption kinetics and thermodynamics of Pd by COF-42, revealing that the adsorption process follows a Freundlich model. The maximum adsorption capacity of COF-42 is 170.6mg/g, demonstrating a superb adsorption capacity for palladium. Additionally, the study also explores the impact of adjusting HNO_3 concentration, and COF-42 dosage on the adsorption performance, highlighting the influence of acidity levels on the final outcome. Lastly, the selectivity of COF-42 towards Pd in the presence of different metal ions and its ability to be reused underscore its effectiveness in Pd(II) adsorption, attributed to the synergistic effects of its flexible ligand, framework porosity, and concentrated –NH/–NH_2 groups with a strong affinity for Pd^{2+}.

Keywords: High-level liquid waste; platinum group metals; COF-42; Palladium; adsorption

1. Introduction

High-Level Liquid Waste (HLLW) is produced along with nuclear power generation that must undergo strict treatment and disposal to prevent environmental and human health risks due to its high radioactivity and toxicity. The current common method for treating HLLW involves glass curing and then placing it underground to isolate it from the environment [1,2]. However, the temperature during the glass curing process is below 1200°C, which is insufficient to melt platinum group metals (PGMs), causing them to accumulate at the bottom of the melting pool and disrupt the furnace's normal operation. Therefore, it is crucial to separate PGMs from HLLW before the glass curing process to guarantee the treatment procedure conducted successfully.

Furthermore, separating PGMs like Pd from HLLW allows for recycling and reuse, offering significant industrial value due to their unique properties and wide-ranging applications in catalytic converters, electronics, pharmaceuticals, and jewelry [3–6]. The demand for PGMs is expected to remain robust in the future. However, the separation of PGMs is a crucial process across various industries, with different methods proposed and utilized, including chemical and physical separation, each with its own set of advantages [7]. By contrast, chemical methods are commonly employed in mining and refining operations to extract PGMs from ores or other materials. Advanced techniques like ion exchange and adsorption are also utilized for precise and efficient PGM separation. Notably, adsorption has emerged as a prominent method due to its simple process, exceptional efficiency (achieving up to 99.9% removal capacity), and low energy consumption

 doi:10.20944/preprints202504.0436.v1

compared to other methods [8]. Various materials such as activated carbon, mesoporous silica, chitosan, and 2D materials have been employed as adsorbents [9–11]. Ideally, an adsorbent should possess a high surface area, excellent stability, and high porosity with specific adsorption sites [12].

Here, covalent organic framework (COF) materials have emerged as a promising option in the realm of adsorption. These materials are recognized as a novel category of crystalline porous substances, with their organic components consisting entirely of light atoms connected by covalent bonds like C-C, C-N, and C-O [13,14]. COFs offer numerous advantages due to their exceptional crystallinity, high porosity, adjustable pore size, ease of processing, and low density [15–17]. These distinctive characteristics empower COFs to efficiently adsorb a variety of molecules and ions. The remarkably low density of COFs stems from their well-organized porous frameworks and light atoms, facilitating their broad utilization in areas such as photoelectricity [18,19], electronic sensing [20–22], catalysis [23], drug delivery [24,25], supercapacitors [26], and adsorption [27–30]. Furthermore, researchers have compiled information on the synthesis, properties, and applications of COFs [31]. Extensive research has been conducted on the adsorption and recovery of metals and organic pollutants including heavy metal ions like Au, Cu, Fe, Pb, Hg, Co, pesticides, dyes, and industrial by-products, shedding light on the adsorption mechanisms involved [12,22,32–35].

Using COF materials for adsorption offers a significant advantage in their ability to selectively capture specific molecules and ions due to their specific affinity within the binding sites. Through precise structural design, researchers can customize COF material properties to target substances, presenting a promising potential for separating molecules and ions under various conditions. Apart from their selectivity, COF materials also demonstrate high adsorption capacities. The extensive surface area of COF materials allows ample space for adsorption, leading to high capacities. This characteristic renders COF materials suitable for diverse applications, ranging from environmental cleanup to gas storage. Additionally, COF materials are recognized for their stability and durability. In contrast to conventional adsorbents that may deteriorate over time, COF materials retain their structure and adsorption capabilities even after numerous adsorption and desorption cycles. This longevity positions COF materials as a cost-efficient and sustainable choice for adsorption purposes.

In this study, a crystalline mesoporous COF material called COF-42 is synthesized *via* a hydrothermal condensation reaction involving 1,3,5-triformylbenzene (TB) and 2,5-diethoxyterephthalohydrazide (DTH). The resulting COF-42 exhibits significant surface area, excellent chemical stability, and enduring porosity, enhancing their efficacy in Pd adsorption under harsh acidic environments.

2. Materials and Method

2.1. Materials

Diethyl 2,5-dihydroxy-terephthalate (96%), 1,3,5-Benzenetricarboxaldehyde (97%) and 1,4-Dioxane ($\geqslant$99.5%) were purchased from Shanghai Aladdin Biochemical Technology Co., Ltd. (Shanghai China). All other regents, such as potassium carbonate, potassium iodide, acetone, ethyl iodide, methanol, methylene chloride, ethanol and hydrazine hydrate were of analytical grade and were used without further purification.

2.2. Preparation of COF-42

The sample of DTH was synthesized according to the previously reported process [36], which can be briefly described as follows. 0.5 g of diethyl 2, 5-dihydroxy-terephthalate, 2 g of potassium carbonate, and 40 mg of potassium iodide were mixed in 40 mL of acetone. Then, 400 mL of ethyl iodide was added, and the mixture was heated and stirred at reflux for 48 hours. After filtration and rinsing the solid residue with hot acetone, a yellow solution was obtained. The solvent was removed by roto evaporation, and the residue was then suspended in water and extracted. The organic extracts were combined, washed with brine, dried, and concentrated by roto evaporation. The resulting solid was purified by recrystallization in methanol. The purified solid was dissolved in 45 mL of ethanol

 doi:10.20944/preprints202504.0436.v1

and 6 mL of hydrazine hydrate, and the mixture was refluxed for 40 hours. Upon cooling, white crystals formed, which were separated by filtration and washed with water and ethanol.

Synthesis of COF-42: A mixture of TB (5 mg) and DHT (18 mg) was combined in a tube containing 250 mL of anhydrous dioxane and 750 mL of mesitylene. The tube was then placed in an ultrasonic bath for 15 minutes. After sonication, 100 mL of 6 M aqueous acetic acid was added. Subsequently, the tube was rapidly frozen at 77 K, evacuated to an internal pressure of 150 m Torr, and heated at 120 ºC for 72 hours. This process resulted in the formation of a pale-yellow solid at the bottom of the tube. The solid was isolated through filtration or centrifugation, washed with anhydrous dioxane and anhydrous acetone, immersed in anhydrous acetone for 24 hours, and finally dried at room temperature and 10^{-2} mTorr for 12 hours, resulting in the production of a pale-yellow powder.

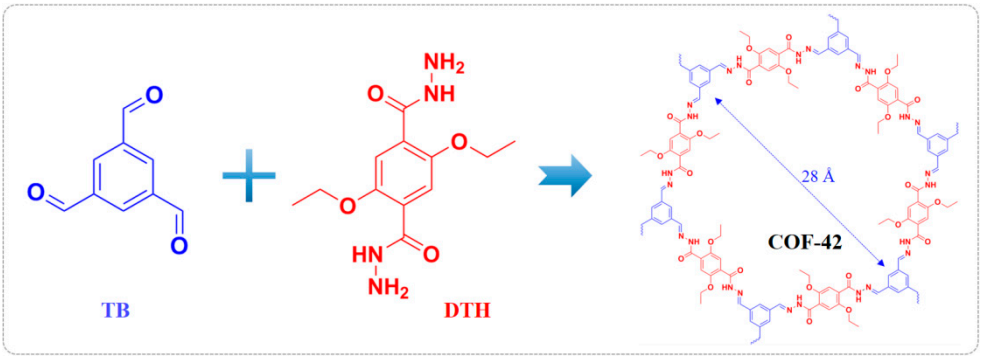

Figure 1. Synthesis of COF-42 by condensation of 2, 5 – diethoxyterephthalohydrazide and 1, 3, 5-Triformylbenzene.

2.3. Adsorption Performance of COF-42 Towards Pd

Prepare a 10 mmol/L metal ion solution, a 5 mol/L HNO_3 solution, and a 5 mol/L $NaNO_3$ solution. Adjust the solution acidity with HNO_3. Combine a specified amount of adsorbent with the metal ion solution in a glass container and place it in a temperature-controlled water bath oscillating at 280 pm. Then, use a syringe filter with a 0.45 m needle for solid-liquid separation, followed by diluting the separated liquid. Analyze the supernatant using ICP-OES to measure the remaining Pd^{2+} content. The partition coefficient (K_d, mL/g) and equilibrium adsorption amount (q_e, mg/g) can be calculated using the equations 1, 2.

$$K_d = \frac{C_i - C_e}{C_e} \times \frac{V}{m} \quad (1)$$

$$q_e = \frac{(C_i - C_e) \times V}{m} \quad (2)$$

where V represents the total solution volume (mL), m is the adsorbent mass (g), C_i and C_e are the initial and equilibrium concentrations of Pd^{2+}, respectively.

2.4. Characterizations

The materials' structure was analyzed using powder X-ray diffraction (PXRD, SmartLab 3KW) with Cu Ka radiation (λ = 1.5406 Å) in the range of 3o to 30º (2θ). Weight changes were tracked through Thermogravimetric Analysis (TGA/DSC3+, Mettler Toledo, Switzerland) with a heating rate of 10º/min at N_2 atmosphere. Scanning electron microscopy (SEM, Hitachi Regulus 8100) combined with energy dispersive X-ray spectroscopy (EDX) was utilized to examine the morphology and elemental distribution. N_2 sorption isotherms were obtained at 77 K using a liquid N_2 bath (Micromeritics/3FLEX). FT-IR spectra were collected using a Nicolet 6700 FTIR spectrometer (Thermo Fisher Scientific). Metal ion concentrations were determined with an Inductively Coupled Plasma

 doi:10.20944/preprints202504.0436.v1

Optical Emission Spectrometer (ICP-OES, JY2000-2) and X-ray photoelectron spectroscopy (XPS) was performed on a Thermo ESCALAB 250.

2.5. Calculations

We have employed the Vienna ab initio simulation package (VASP)37 to perform all density functional theory (DFT) calculations within the generalized gradient approximation (GGA) using the Perdew-Burke-Ernzerhof (PBE)38 formulation. We have chosen the projected augmented wave (PAW) potentials39 to describe the ionic cores and take valence electrons into account using a plane wave basis set with a kinetic energy cutoff of 450eV. Partial occupancies of the Kohn−Sham orbitals were allowed using the Gaussian smearing method and a width of 0.05 eV. The electronic energy was considered self-consistent when the energy change was smaller than $10-5$eV. A geometry optimization was considered convergent when the force change was smaller than 0.05 eV/Å. Grimme's DFT-D3 methodology40 was used to describe the dispersion interactions. The Brillourin zone was sampled with a gamma-centered grid $1\times1\times1$ through all the computational process. Periodic boundary conditions were used in all directions and a vacuum layer of 15 Å was used in the z-direction to separate the slabs.

The adsorption energy (Eads) of adsorbate molecule was defined as

$$E_{ads} = E_{mol/surf} - E_{surf} - E_{mol} \quad (3)$$

where $E_{mol/surf}$, E_{surf} and E_{mol} are the energy of adsorbate molecule adsorbed on the surface, the energy of clean surface, and the energy of molecule respectively.

3. Result and Discussion

3.1. The Characterization of COF-42

The nitrogen adsorption isotherm of COF-42 is analyzed at 77 K to determine the surface and pore characteristics. The isotherm displays distinct adsorption behavior below P/P°=0.04, with a noticeable step between P/P°=0.04-0.18. The N_2 adsorption-desorption isotherm exhibits a narrow hysteresis loop, indicating a type-IV isotherm with mesoporous features. The BET surface area is notably high at 614.8 m^2/g (**Fig.2a**), while the average pore diameter is calculated and measured at 2.6 nm (**Fig.2b**).

The crystallinity of the COF-42 sample is assessed using Powder X-ray diffraction (PXRD). The diffraction peaks at 2θ=3.2° (27.59 Å), 2θ=7.3° (12.10 Å), and 2θ=9.1° (9.71 Å) corresponded to the (100), (200), and (210) crystal planes, respectively (**Fig.2c**) [22,36]. The lattice spacing *d* is calculated by the Bragg equation. These results indicate that the synthesized COF-42 is integrated and possesses high crystallinity, a crucial factor for its superior performance in adsorption applications.

The excellent stability and integrity of COF-42 are validated through TGA depicted in **Fig.2d**. The analysis revealed a minor weight loss (~6.5%) below 320°C, attributed mainly to the evaporation of water and organic solvents within the COF-42 structure 41. This indicates that the structure of COF-42 can remain thermal stable at high temperatures, which is very important for its diverse applications. Subsequently, a significant weight loss (~43.1%) occurs between 320°C and 550°C, likely due to the thermal decomposition of functional groups on the COF-42 framework. Any further weight loss above 550°C is resulted from the additional pyrolysis of the COF-42 framework itself.

 doi:10.20944/preprints202504.0436.v1

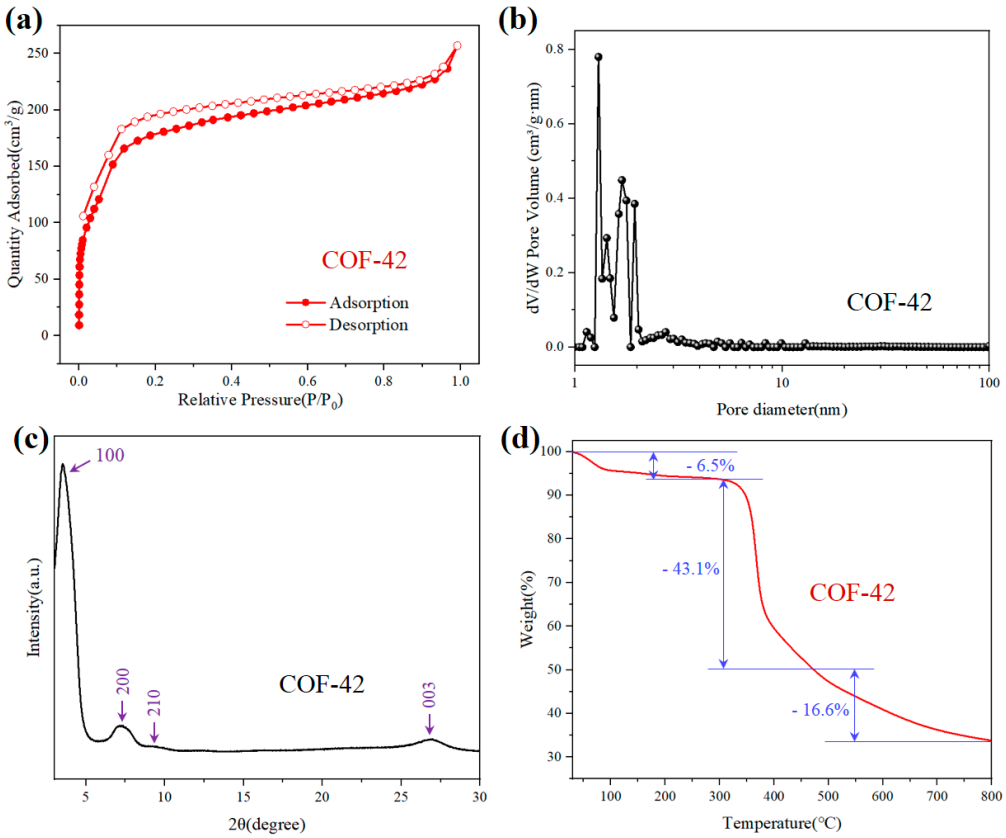

Figure 2. (a) N_2 sorption isotherm and (b) pore size distribution of COF-42 measured at 77 K. (c) PXRD patterns and (d) TGA data of COF-42.

3.2. The Sorption Performance of COF-42 Towards Pd(II)

After confirming the COF-42 structure, the dynamics of COF-42 towards Pd adsorption are further studied. Firstly, the adsorption isotherm is determined using 5 mg of COF-42 at room temperature in a 3M HNO_3 solution. The adsorption isotherm represents the relationship between adsorption capacity and the equilibrium concentration of metal ions by altering the concentration of single metal ions at a specific temperature. Typically, there are two main models used to fit the adsorption isotherm curves. The Langmuir model describes adsorption sites that are uniformly distributed with equal capacity, following a monolayer adsorption mechanism. On the other hand, the Freundlich model suggests surfaces with heterogeneous adsorption, featuring varying adsorption energies 42. The Langmuir and Freundlich models are expressed by specific equations.

$$\text{Langmuir model}: \frac{C_e}{q_e} = \frac{1}{q_{max} K_L} + \frac{C_e}{q_{max}} \tag{4}$$

$$\text{Freundlich model}: \log q_e = \log K_F + \frac{1}{n} \log C_e \tag{5}$$

where, q_e and q_m represent the equilibrium and theoretical saturation adsorption capacities of the adsorbent in millimoles per gram (mg/g), respectively; C_e stands for the equilibrium adsorption concentration of metal ions in millimoles per liter (mg/L); K_L (L/mg) and K_F (mg/g) are the Langmuir and Freundlich model constants, respectively; n indicates the adsorption strength. Thus, the fitted results are completed using the Langmuir and Freundlich models as shown in **Fig.3a** and **Table S1**. The isotherm fitting with the Langmuir model showed a higher correlation coefficient (reaching 99.7%), suggesting that the adsorption process of Pd on COF-42 is uniformly distributed with equal capacity and monolayer adsorption. Moreover, COF-42 exhibited a high saturation adsorption

 doi:10.20944/preprints202504.0436.v1

capacity of approximately 170.6 mg/g at 298K, attributed to the abundant accessible Pd adsorption sites distributed across the channel surface of COF-42.

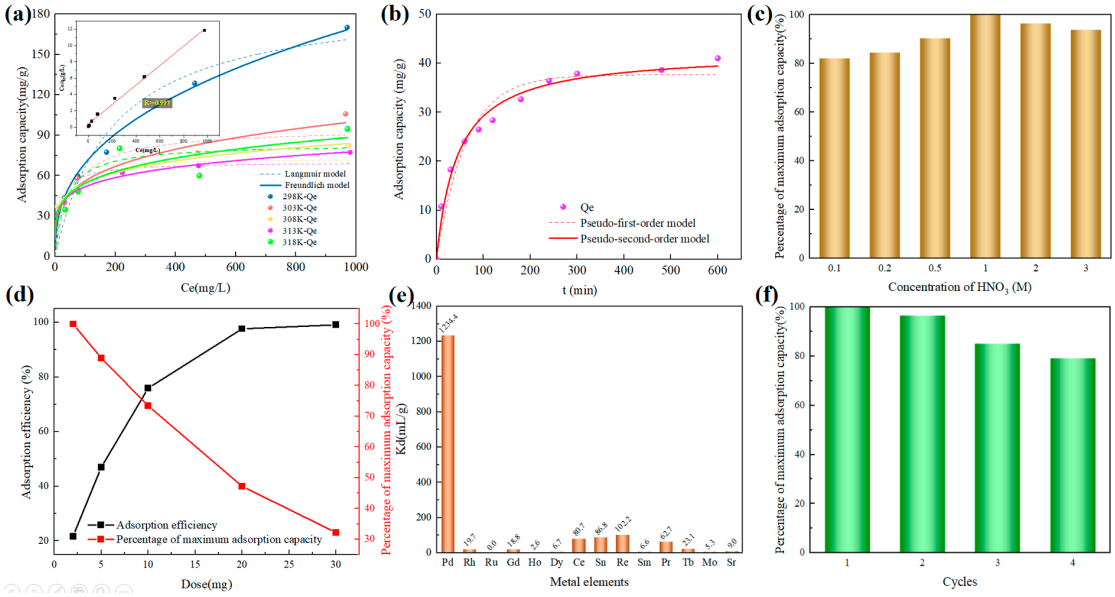

Figure 3. (a) Adsorption isotherm of COF-42 towards Pd^{2+}. Inset is the fitted line by using the Langmuir adsorption model. (b) Adsorption kinetic results of COF-42 towards Pd^{2+} versus time. (c) Effect of (d) HNO_3 concentration and (d) COF-42 dose on the Pd^{2+} adsorption of COF-42. (e) The adsorption capacity of COF-42 towards various ions. (f) The reusability of COF-42.

The adsorption capacity of COF-42 for Pd^{2+} in a 3M HNO_3 solution is evaluated through the analysis of experimental data using quasi-first-order and quasi-second-order kinetic models, as depicted in **Fig.3b**. The equations are represented as:

$$\ln(q_e - q_t) = \ln q_t - k_1 t \tag{6}$$

$$\frac{t}{q_t} = \frac{1}{k_2 q_e^2} + \frac{t}{q_e} \tag{7}$$

Here, k_1 (min^{-1}) and k_2 (g mg^{-1} min^{-1}) denote the pseudo-first-order rate constant and pseudo-second-order rate constant of adsorption, respectively. q_t (mg g^{-1}) indicates the amount of Pd^{2+} adsorbed at time t (min), while q_e (mg g^{-1}) represents the equilibrium amount of Pd^{2+} adsorbed 43.

The results of the fitting are shown in **Table S2**, indicating that the adsorption kinetics align well with the pseudo-second-order kinetic model due to the coefficient of determination R^2 being close to 1. Furthermore, the calculated equilibrium adsorption capacity closely approximates the experimental results compared to the quasi-first-order kinetic calculations. Therefore, the chemical reaction is the controlling step in the adsorption process. The initial adsorption rate is represented by $k_2 q_e^2$, where 92.36% of the adsorption capacity can be attained within 300 minutes, leading to equilibrium. The relatively fast kinetics observed in COF-42 can be attributed to the high concentration of -NH/-NH_2 species and a significant number of ordered pore channels that enhance the diffusion of Pd^{2+} ions. After an extended contact time of 10 hours, the Pd^{2+} concentration fell below the detection limit of ICP-OES. These results emphasize the effectiveness of using COFs as promising candidates for the removal of Pd^{2+} from HNO_3 conditions.

By varying the concentration of HNO_3, the adsorption capacities of COF-42 under different acidity levels are investigated to analyze the influence of acid on the adsorption process of COF-42 towards Pd. The results show that the adsorption capacity of COF-42 increased initially with acidity and then decreased, reaching its maximum at 1 M HNO_3 (**Fig.3c**). When the concentration of nitric acid in the solution is 3M, the adsorption capacity can still reach 93.8% of the maximum adsorption

 doi:10.20944/preprints202504.0436.v1

capacity. This indicates that compared to other COF materials, COF-42 exhibits better acid resistance and material stability, with its adsorption capacity varying by less than 10% with changes in acidity.

Moreover, as depicted in **Fig.3d**, the adsorption capacity changes along with the solid-to-liquid ratio, and the experiment is conducted at room temperature under 3M acidity. With the COF-42 dosage increasing from 2mg to 20mg, the Pd adsorption rate rose from 21.71% to 97.62%. When the COF-42 dosage increased from 20mg to 30mg, the adsorption rate increased from 97.62% to 99.07%. This indicates that the adsorption of Pd tends towards saturation, with the adsorption rate nearing 100%.

Selectivity plays a crucial role in the recovery of Pd from a given solvent containing various metal ions. To assess COF-42's capability in removing Pd under practical conditions, a study is conducted at room temperature with a 3M HNO_3 solution to investigate the metal ion adsorption selectivity of COF-42, as illustrated in **Fig. 3e**. Under identical conditions, Pd exhibited notably high adsorption when interacting with COF-42 while showing minimal adsorption of other ions such as Rh, Ru, Gd, Ho, Dy, Ce, Sn, Re, Sm, Pr, Tb, Mo, and Sr. This distinct selectivity of COF-42 is attributed to its chelating groups based on –NH/–NH_2. Actually, the exceptional adsorption performance of COF-42 towards Pd^{2+} is explained by a synergistic effect resulting from a flexible ligand, framework porosity, and concentrated –NH/–NH_2 groups with a strong affinity for Pd^{2+}. The presence of accessible –NH/–NH_2 sites within the channels of COF-42 further boosts its adsorption capacity for Pd^{2+}, underscoring its significant potential for Pd removal.

Further experiments are conducted on COF-42 under conditions of acidity of 3M and a metal ion concentration of 0.05 g/L for repeated use. Initially, 5mg of COF-42 is added to a 10mL centrifuge tube, then incubated at 25°C in a shaker for 20 hours. The supernatant is obtained by centrifugation, and the metal ion concentration is measured by ICP-OES. The remaining COF-42 solid is added to thiourea, placed in a constant temperature shaking incubator, and shaken at 25°C for 24 hours. After centrifugation and washing with distilled water, a second adsorption test is conducted. This process is repeated 4 times. Although there is a slight decrease in the adsorption and desorption capacity of Pd^{2+} after four repetitions (~80% retention), the difference is not significant. Moreover, the use of only 5mg of adsorbent and some loss during adsorption and desorption steps had a considerable impact. Consequently, COF-42 materials with –NH/–NH_2 exhibit a high potential for Pd adsorption capacity and selectivity, coupled with their excellent recyclability, making them valuable for a variety of applications.

COF-42 is recognized as a superior Pd adsorption material due to its mesoporous channels and high crystallinity. Additionally, the designed –NH/–NH_2 species in this study are noted for their remarkable binding interactions with Pd, enhancing the adsorption performance towards Pd. To elucidate the adsorption mechanism, FTIR, XPS and SEM spectra are measured and analyzed before and after Pd adsorption in the subsequent investigation.

3.3. The Sorption Mechanism of COF-42

To further analyze the adsorption mechanism of COF-42 towards Pd, the FT-IR, XPS, SEM images and elemental distributions of COF-42 before and after Pd adsorption are comprehensively studied. The results confirmed the successful copolymerization of the raw materials and Pd binding interaction. The FT-IR spectra in **Fig. 4a** show peaks in the range of 4000-480 cm^{-1}. Specific peaks at 1614 cm^{-1} and 1215 cm^{-1} correspond to $\upsilon_{C=N}$ moiety stretching modes, while the $\upsilon_{C=O}$ band in the COF structure is at 1663 cm^{-1} 44. Notably, no signals for carbonyl $\upsilon_{C=O}$ stretching modes of aldehyde groups in the starting materials were detected in the COFs' FT-IR spectra 36. The appearance of a new peak at 1615 cm^{-1} indicates the successful formation of imine bonds [33]. Furthermore, after Pd adsorption, a new peak at 1380 cm^{-1} emerged, attributed to NO_3^- adsorption from HNO_3 in the material.

 doi:10.20944/preprints202504.0436.v1

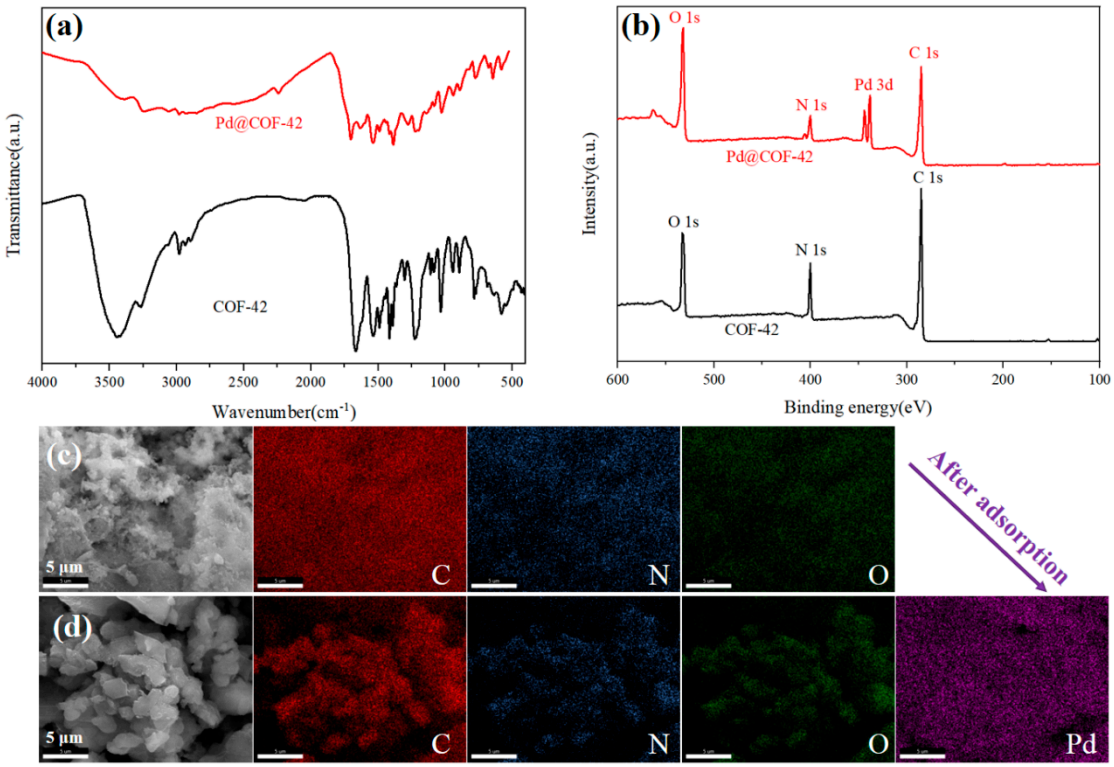

Figure 4. (a) FT-IR and (b) XPS spectra of COF-42 and Pd@COF-42. SEM images and elements distribution of (c) COF-42 and (d) Pd@COF-42.

Furthermore, the XPS analysis of COF-42 and Pd@COF-42 is presented in **Fig. 4b and Fig. 5**. The clear peaks of O1s, N1s, and C1s are observed in COF-42. Additionally, the emergence of new Pd3d peaks post Pd adsorption signifies effective Pd adsorption with robust affinity and chemisorption capabilities (**Fig. 4b and Fig. 5e**). After adsorption of palladium, a new peak of N1s in Pd@COF-42 appeared (**Fig. 5a, c**), with a peak of 405.8 eV considered to be the nitrate group and a peak of 401.4 eV considered to be N-Pd. Comparing the fits before and after adsorption, it can be assumed that the -NH/-NH_2 group contributes to the adsorption of palladium, especially the -NH group. Particularly, the pronounced Pd with N1s peak compared to Pd with O1s suggests a stronger interaction between Pd and N species in a harsh HNO_3 environment, forming a complex involving NO_3^- to maintain charge equilibrium. This establishes Pd^{2+} coordination with the N site through a coordination mechanism, affirming the high crystalline and stable structure of COF-42.

The SEM images show that COF-42 is composed of microparticles (**Fig. 4c**). Following Pd adsorption (**Fig. 4d**), a noticeably large structure is observed, likely due to a significant amount of Pd being adsorbed within the building channels of COF-42. EDX analysis indicates a uniform distribution of the main elements (C, N, O) in the COF-42 structure both before and after Pd adsorption, suggesting successful copolymerization and structural stability during the adsorption process. Additionally, the even distribution of Pd on the surface of Pd@COF-42 demonstrates effective Pd adsorption on the COF-42 structure, with no visible agglomeration occurring.

 doi:10.20944/preprints202504.0436.v1

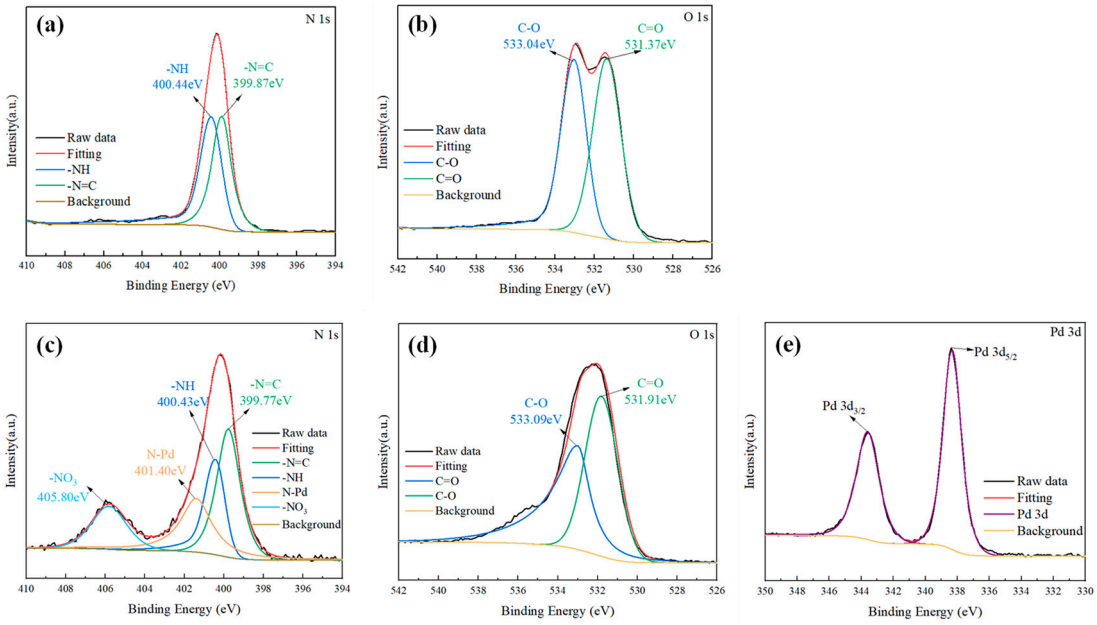

Figure 5. XPS spectra of N1s (a, c), O1s (b, d) and Pd3d (e) for COF-42 and Pd@COF-42.

To investigate the interaction mechanism between Pd(II) and COF-42, the binding energy was determined through density functional theory (DFT) calculations. DFT offers a simple and flexible approach to evaluate the binding energies and electron density distribution of atoms and molecules, enabling a deeper understanding of interactions and facilitating predictions of reaction behavior. As illustrated in **Fig. 6**, the binding energy between Pd(II) and COF-42 was calculated using DFT. The results show that the binding energies of -$Pd(NO_3)_2$ with N atoms are -1.75 eV, and with O atoms are -1.67 eV. These relatively high binding energies indicate the existence of strong interactions, suggesting that -$Pd(NO_3)_2$ tends to preferentially adsorb on N atoms. The negative binding energies highlight the existence of substantial chemical binding interactions, resulting in enhanced adsorption stability.

Integrating the results from characterizations and DFT analysis, it is evident that COF-42 exhibits a strong and stable adsorption mechanism. This can be primarily attributed to the abundance of active nitrogen (N) sites distributed across its surface. These active N sites serve as key coordination centers, facilitating strong interactions with Pd(II) ions through chemical bonding. The coordination interaction not only enhances the adsorption strength but also imparts high selectivity towards Pd(II), ensuring that the material preferentially adsorbs the target ions even in the presence of competing species. This selectivity is critical for applications in complex environments, such as wastewater treatment or resource recovery.In addition to its chemical affinity for Pd(II), the structural properties of COF-42 play a vital role in its adsorption performance. The material's high surface area provides ample space for ion access, while its large porosity promotes efficient mass transfer and diffusion of Pd(II) ions into the interior adsorption sites. The interconnected porous network ensures that ions can be rapidly transported to active sites, improving adsorption kinetics.

 doi:10.20944/preprints202504.0436.v1

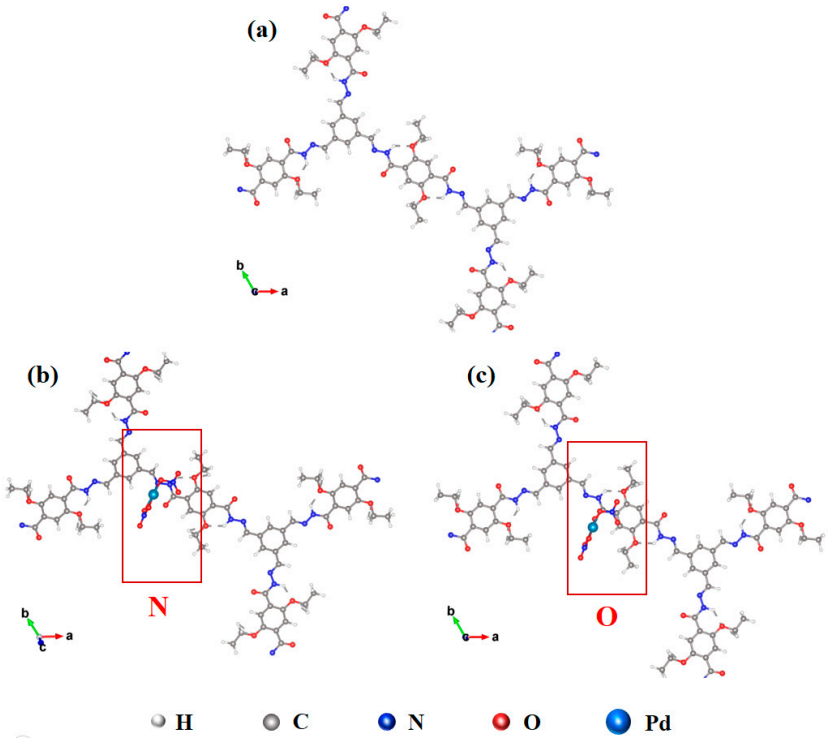

Figure 6. (a) DFT calculations of COF-42 and -Pd(NO$_3$)$_2$ with (b) *N* and (c) O on Pd@COF-42 structure.

4. Conclusion

To summarize, this study successfully constructs a well-defined 2D porous COF-42 and applied it to effectively adsorb Pd^{2+}. The structure and morphology of COF-42 are measured before and after Pd adsorption, indicating high integrity and stability. The analysis of adsorption dynamics and thermodynamics show that the process followed a pseudo-second-order kinetic model and Langmuir model. The maximum adsorption capacity at 3M HNO_3 solution was 170.6 mg/g, and the adsorption equilibrium could be reached within 300 minutes. The exceptional adsorption performance is attributed to the synergistic effect of flexible ligand, framework porosity, and concentrated -NH/-NH_2 groups of COF-42, which exhibited a strong affinity for Pd^{2+}. Therefore, COF-42 demonstrated excellent capture efficiency towards Pd ions in a strong acid environment, indicating its potential application in Pd adsorption and recycling.

Supplementary Materials: The following supporting information can be downloaded at the website of this paper posted on Preprints.org.

Acknowledgments: This work was financially supported by National Natural Science Foundation of China (U2067212).

References

1. Järvine AK, Murchison AG, Keech PG et al (2020) A probabilistic model for estimating the life expectancy of used nuclear fuel containers in a canadian geological repository: effects of latent defects and repository temperature. Nucl Technol 206 (7):1036–1058.
2. Shiwei Yu, Junze Zhang, Ke Ling, Lianghua Han & Lie Liu, Rapid vitrification of simulated HLLW by ultra-high power laser, Journal of Radioanalytical and Nuclear Chemistry, https://doi.org/10.1007/s10967-024-09467-w
3. Iakovos Yakoumis, Marianna Panou, Anastasia Maria Moschovi, Dimitris Panias, Recovery of platinum group metals from spent automotive catalysts: A review, Cleaner Engineering and Technology, 2021, 3, 100112.

 doi:10.20944/preprints202504.0436.v1

4. Huimin Tang, Zhiwei Peng 1, Ran Tian, Lei Ye, Jian Zhang, Mingjun Rao, Guanghui Li, Platinum-group metals: Demand, supply, applications and their recycling from spent automotive catalysts, Journal of Environmental Chemical Engineering, 2023, 11, 110237.
5. Ashish Pathak, Hanadi Al-Sheeha, R. Navvamani, Richa Kothari, Meena Marafi & Mohan S. Rana, Recycling of platinum group metals from exhausted petroleum and automobile catalysts using bioleaching approach: a critical review on potential, challenges, and outlook, Reviews in Environmental Science and Bio/Technology, 2022, 21, 1035–1059.
6. Jinsong Xia, Ahmad Ghahreman, Platinum group metals recycling from spent automotive catalysts: metallurgical extraction and recovery technologies, Separation and Purification Technology, 2023, 311, 123357.
7. Huandong Zheng, Yunji Ding, Quan Wen, Bo Liu, Shengen Zhang, Separation and purification of platinum group metals from aqueous solution: Recent developments and industrial applications, Resources, Conservation and Recycling, 2021, 167, 105417.
8. Huang N, Zhai L, Xu H, Jiang D (2017) Stable covalent organic frameworks for exceptional mercury removal from aqueous solutions. J Am Chem Soc 139:2428–2434.
9. Leandro Pellenz, Carlos Rafael Silva de Oliveira, Afonso Henrique da Silva Júnior, Layrton José Souza da Silva, Luciano da Silva, Antônio Augusto Ulson de Souza, Selene Maria de Arruda Guelli Ulson de Souza, Fernando Henrique Borba, Adriano da Silva, A comprehensive guide for characterization of adsorbent materials, Separation and Purification Technology, 2023, 305, 122435.
10. Shihai Xu, Chuncai Zhou, Hongxia Fang, Wenrui Zhu, Jiaqian Shi, Guijian Liu, Synthesis of ordered mesoporous silica from biomass ash and its application in CO2 adsorption, Environmental Research, 2023, 231, 116070.
11. Pankaj Bhatt, Samiksha Joshi, Gulsum Melike Urper Bayram, Priyanka Khati, Halis Simsek, Developments and application of chitosan-based adsorbents for wastewater treatments, Environmental Research, 2023, 226, 115530.
12. Eman Abdelnasser Gendy, Daniel Temitayo Oyekunle, Jerosha Ifthikar, Ali Jawad, Zhuqi Chen, A review on the adsorption mechanism of different organic contaminants by covalent organic framework (COF) from the aquatic environment, Environmental Science and Pollution Research (2022) 29:32566–32593.
13. C. S. Diercks and O. M. Yaghi, Science, 2017, 355, 923.
14. San-Yuan Ding, Xiao-Hui Cui, Jie Feng, Gongxuan Lu and Wei Wang, Facile synthesis of –CQN– linked covalent organic frameworks under ambient conditions, Chem. Commun., 2017, 53, 11956.
15. Chen, X.; Geng, K.; Liu, R.; Tan, K. T.; Gong, Y.; Li, Z.; Tao, S.; Jiang, Q.; Jiang, D. Covalent Organic Frameworks: Chemical Approaches to Designer Structures and Built-In Functions. Angew. Chem., Int. Ed. 2020, 59, 5050−5091.
16. Guan, X.; Chen, F.; Fang, Q.; Qiu, S. Design and Applications of Three Dimensional Covalent Organic Frameworks. Chem. Soc. Rev. 2020, 49, 1357−1384.
17. Evans, A. M.; Parent, L. R.; Flanders, N. C.; Bisbey, R. P.; Vitaku, E.; Kirschner, M. S.; Schaller, R. D.; Chen, L. X.; Gianneschi, N. C.; Dichtel, W. R. Seeded growth of single-crystal two-dimensional covalent organic frameworks. Science 2018, 361, 52−57.
18. H. Liao, H. Ding, B. Li, X. Ai and C. Wang, J. Mater. Chem. A, 2014, 2, 8854.
19. Liang Zhang, Lezhi Yi, Zhi-Jun Sun, Hexiang Deng, Covalent organic frameworks for optical applications, Aggregate. 2021;2: e24.
20. Ding, X.; Guo, J.; Feng, X.; Honsho, Y.; Guo, J.; Seki, S.; Maitarad, P.; Saeki, A.; Nagase, S.; Jiang, D. Angew. Chem., Int. Ed. 2011, 50, 1289–1293.
21. S.-Y. Ding, M. Dong, Y.-W. Wang, Y.-T. Chen, H.-Z. Wang, C.-Y. Su and W. Wang, J. Am. Chem. Soc., 2016, 138, 3031.
22. Ali Reza Zanganeh, COF‑42 as sensory material for voltammetric determination of Cu(II) ion: optimizing experimental condition via central composite design, Journal of Applied Electrochemistry (2022) 53:765–780
23. Sun, Q.; Aguila, B.; Perman, J.; Nguyen, N.; Ma, S. Flexibility Matters: Cooperative Active Sites in Covalent Organic Framework and Threaded Ionic Polymer. J. Am. Chem. Soc. 2016, 138 (48), 15790−15796.

 doi:10.20944/preprints202504.0436.v1

24. Q. Fang, J. Wang, S. Gu, R. B. Kaspar, Z. Zhuang, J. Zheng, H. Guo, S. Qiu and Y. Yan, J. Am. Chem. Soc., 2015, 137, 8352.
25. Mitra, S.; Sasmal, H. S.; Kundu, T.; Kandambeth, S.; Illath, K.; Diaz Diaz, D.; Banerjee, R. Targeted Drug Delivery in Covalent Organic Nanosheets (CONs) via Sequential Postsynthetic Modification. J. Am. Chem. Soc. 2017, 139 (12), 4513−4520.
26. Khayum M, A.; Vijayakumar, V.; Karak, S.; Kandambeth, S.; Bhadra, M.; Suresh, K.; Acharambath, N.; Kurungot, S.; Banerjee, R. Convergent Covalent Organic Framework Thin Sheets as Flexible Supercapacitor Electrodes. ACS Appl. Mater. Interfaces 2018, 10 (33), 28139-28146.
27. Doonan, C. J.; Tranchemontagne, D. J.; Glover, T. G.; Hunt, J. R.; Yaghi, O. M. Nat. Chem. 2010, 2, 235–238.
28. M. G. Rabbani, A. K. Sekizkardes, Z. Kahveci, T. E. Reich, R. Ding and H. M. El-Kaderi, Chem. – Eur. J., 2013, 19, 3324.
29. Zhifang Wang, Qi Yu, Yubo Huang, Hongde An, Yu Zhao, Yifan Feng, Xia Li, Xinlei Shi, Jiajie Liang, Fusheng Pan, Peng Cheng, Yao Chen, Shengqian Ma, and Zhenjie Zhang, PolyCOFs: A New Class of Freestanding Responsive Covalent Organic Framework Membranes with High Mechanical Performance, ACS Cent. Sci. 2019, 5, 1352−1359.
30. Nada Elmerhi, Sushil Kumar, Maguy Abi Jaoude, and Dinesh Shetty, Covalent Organic Framework-derived Composite Membranes for Water Treatment, Chem Asian J. 2024, 19, e202300944.
31. Tiago F. Machado, M. Elisa Silva Serra, Dina Murtinho, Artur J. M. Valente and Mu. Naushad, Covalent Organic Frameworks: Synthesis, Properties and Applications—An Overview, Polymers 2021, 13, 970.
32. R. Xue, H. Guo, T. Wang, L. Gong, Y. Wang, J. Ai, D. Huang, H. Chen and W. Yang, Anal. Methods, 2017, 9, 3737–3750.
33. Zhiming Zhou, Wanfu Zhong, Kaixun Cui, Zanyong Zhuang, Lingyun Li, Liuyi Li, Jinhong Bi and Yan Yu, A covalent organic framework bearing thioether pendant arms for selective detection and recovery of Au from ultra-low concentration aqueous solution, Chem. Commun., 2018, 54, 9977–9980.
34. Zarifeh Raji, Ahasanul Karim, Antoine Karam and Seddik Khalloufi, Adsorption of Heavy Metals: Mechanisms, Kinetics, and Applications of Various Adsorbents in Wastewater Remediation—A Review, Waste, 2023, 1, 775–805. https://doi.org/10.3390/waste1030046.
35. Yuhuan Feia and Yun Hang Hu, Design, synthesis, and performance of adsorbents for heavy metal removal from wastewater: a review, J. Mater. Chem. A, 2022, 10, 1047-1085.
36. Fernando J. Uribe-Romo, Christian J. Doonan,| Hiroyasu Furukawa, Kounosuke Oisaki, and Omar M. Yaghi, Crystalline Covalent Organic Frameworks with Hydrazone Linkages, J. Am. Chem. Soc. 2011, 133, 11478–11481.
37. Kresse, G.; Furthmüller, J. Efficiency of Ab-Initio Total Energy Calculations for Metals and Semiconductors Using a Plane-Wave Basis Set. Comput. Mater. Sci. 1996, 6, 15−50.
38. Perdew, J. P.; Burke, K.; Ernzerhof, M. Generalized Gradient Approximation Made Simple. Phys. Rev. Lett. 1996, 77, 3865−3868.
39. Kresse, G.; Joubert, D. From Ultrasoft Pseudopotentials to the Projector Augmented-Wave Method. Phys. Rev. B 1999, 59, 1758-1775.
40. Grimme, S.; Antony, J.; Ehrlich, S.; Krieg, H. J. Chem. Phys. 2010, 132, 154104.
41. Austin M. Evans, Matthew R. Ryder, Woojung Ji, Michael J. Strauss, Amanda R. Corcos, Edon Vitaku, Nathan C. Flanders, Ryan P. Bisbey and William R. Dichtel, Trends in the thermal stability of two-dimensional covalent organic frameworks, Faraday Discuss., 2021,225, 226-240.
42. Jianlong Wang, Xuan Guo, Adsorption isotherm models: Classification, physical meaning, application and solving method, Chemosphere, 2020, 258, 127279.

 doi:10.20944/preprints202504.0436.v1

43. Jianlong Wang, Xuan Guo, Adsorption kinetic models: Physical meanings, applications, and solving methods, Journal of Hazardous Materials, 2020, 390, 122156.
44. Uribe-Romo, F. J.; Hunt, J. R.; Furukawa, H.; Klöck, C.; O'Keeffe, M.; Yaghi, O. M. J. Am. Chem. Soc. 2009, 131, 4570–4571.